Desalination and Water Treatment
www.deswater.com

doi: 10.5004/dwt.2018.22155

112 (2018) 282–291
April

Effects of membrane envelope geometry on hydrodynamics inside draw channel of forward osmosis spiral wound membrane element

Chulmin Lee[a], Seungho Kook[a], Changkyoo Choi[b], Thanh-Tin Nguyen[a], In S. Kim[b,*]

[a]*School of Earth Sciences and Environmental Engineering, Gwangju Institute of Science and Technology (GIST), 123 Cheomdangwagi-ro, Buk-gu, Gwangju, 61005, Korea*
[b]*Global Desalination Research Center, Gwangju Institute of Science and Technology (GIST), 123 Cheomdangwagi-ro, Buk-gu, Gwangju, 61005, Korea, Tel. +82-62-715-2436; email: iskim@gist.ac.kr (I.S. Kim)*

Received 19 December 2017; Accepted 15 January 2018

ABSTRACT

Forward osmosis spiral wound membrane (SWM) element has a modified envelope geometry equipped with central glue line and blocked central tube to accommodate forward osmosis process. Due to modified module structure, water channel inside modified SWM element creates unique flow behaviors and affects performance of modified SWM element. However, research on this issue is severely limited in the current stage. Several studies used two-dimensional simulation approaches on this modified SWM element envelope geometry; however, three-dimensional simulation considering effects of spacer-filled channel has not been performed yet. This study employs three-dimensional computational fluid dynamics to investigate effects of different ratio between length and width of membrane envelope and central glue line length and envelope length. Various hydrodynamic parameters such as Reynolds number, power number, Fanning friction factor, and wall shear rate were calculated and compared. Simulation results showed that short and wide envelope geometry is more advantageous for low energy consumption while narrow and long envelope geometry induce higher wall shear rate.

Keywords: Computational fluid dynamics; Forward osmosis; Spiral wound element; Spacer-filled channel; Hydrodynamics

1. Introduction

Forward osmosis (FO) has attracted much attention from both academic and industrial fields as an emerging membrane separation technology during the past decades. This research concentration on FO technology is due to several advantages over other membrane technologies such as low capital cost, low operating cost, and less problematic fouling issues [1]. Most of all, the reverse osmosis (RO) process, which is dominant technology in the industry during the last 40 years, has significantly improved its energy efficiency and reached its saturation point. In the research circles, therefore, it is now understood that, the opportunity for further significant reduction in energy consumption for the RO process is slim, whereas FO is expected to address shortcomings of existing pressure-driven membrane processes [1–3].

Among several types of membrane modules, spiral wound membrane (SWM) element is the most commonly used and has dominated desalination membrane market for several decades since its origination. With the development of membrane technology, there have been numerous studies investigated on geometric features of SWM and how they affect the hydrodynamics inside modules and membrane performances [4–7]. There could be a number of geometric factors affecting performance of SWM module but most of them fall into the following categories: the geometry of the membrane envelopes (length, width, and the number of envelopes), channel heights (spacer filaments thickness), spacer's orientation, shape, dimensions, and mesh [4].

* Corresponding author.

Presented at the 10th International Desalination Workshop (IDW 2017), November 22–25, 2017, Busan, Korea.

An SWM element is typically used for the RO and ultrafiltration process and is manufactured by winding the flat sheet membranes around a perforated central pipe. As FO technology was introduced to desalination research field since early 90s, this SWM was modified to accommodate FO process. Because of complexity of FO process, structures of FO SWM are modified with additional structural features. Central pipe is blocked at the center, and center glue line (GL) is inserted into the membrane envelope, which divert the draw solution along flow path induced by center GL and blocked central pipe. During its transit of the draw channel, the draw solution is diluted by osmotically pulling water through the membranes from the feed solution.

Regarding modified FO SWM element, there have been several papers attempted to analyze mass transfer and membrane performance associated with membrane envelope geometry. Jung et al. [8] evaluated the FO membrane performance, permeate flux, and recovery rate depending on membrane orientation, flow direction of feed and draw solutions, flow rate, and solute resistivity using two-dimensional (2D) FO simulation. Gu et al. [9] carried out simulations for a comparison between FO plate and frame and modified SWM module with varying four types of operating conditions: volumetric flow rate of the feed and the draw solution, the concentration of the draw solution, flow direction, and the membrane orientation. However, due to inherent limitation of 2D simulation approach, above studies are limited to 2D mass balance equations and only the dominant flow direction is considered which does not take into consideration of the effects of spacer and the associated complex flow behaviors.

Researchers in the field of membrane science using computational fluid dynamics (CFD) tools for flow visualization through membrane module have generally made the assumption that the flow through a spacer-filled rectangular channel is a good representation of the flow in case of SWM elements having similar spacer in the feed channel. This assumption was first validated experimentally by Schock and Miquel [10] and later by Ranade and Kumar [11,12] using a periodic unit cell approach. Most studies have followed this so-called, "unit cell" approach, however, in case of modified SWM element, this approach is not applicable. In draw channel of modified SWM envelope, the flow direction is not constant but changes along the flow path set by blocked central tube and central GL. In this case, periodic or symmetric boundary condition is not appropriate to use because it violates the assumption of unit cell approach which is flow direction has to be constant while flowing and side wall effect is negligibly small. In this study, therefore, a single unit cell approach will be extended to "envelope unit approach" to address this issue.

The objective of this paper is to investigate effects of geometric features of FO-modified SWM envelope based on various hydrodynamic parameters that dictate energy consumption and hydrodynamics inside water channel of specific envelope unit. To the best of the authors' knowledge, this is the first study to investigate hydrodynamics of FO SWM element envelope draw channel with considering presence of spacers in three-dimensional (3D) coordinate system. The approach and results presented in this work will have significant implications for elucidating the relationship between modified SWM envelope geometry and membrane performance. This study also suggests important design factors such as ratio of envelope length and width, central GL, and envelope length of FO SWM element membrane envelope and element.

2. Simulation approach

2.1. Envelope geometric conditions and boundary conditions

In the current simulations, 15 envelope geometries with different geometrical features have been studied. For geometrical features to be compared based on hydrodynamic parameters, length–width (LW) ratio and GL ratio have been used. LW ratio and GL ratio are defined as proportion of envelope length to envelope width and the proportion of center GL length to envelope length, respectively. They will be referred to as "GL ratio" and "LW ratio" in the following sections. Ranges of 0.67–3 and 0.1–0.9 for LW ratio and GL ratio were used in current simulations. In order to compare geometries with different LW ratio, envelope area and inlet flow velocity have been kept constant while envelope length and width have been adjusted according to each LW ratio. In this way, hydrodynamics in each geometry can be compared exclusively depending on its ratio of envelope length and width under identical condition of membrane surface area and hydrodynamics.

Existing studies on hydrodynamics inside SWM spacer-filled channel occasionally used Reynolds number to facilitate the comparison of results to identify effects of different geometrical features in SWM water channels. However, for practical flow velocity condition of modified SWM element draw channel, inlet velocity condition was chosen as 6 L/min from literature regarding FO SWM pilot [13,14] and modified according to geometrical features of modified SWM element used in the literature. The inlet velocity condition is determined using the equation below:

$$u_0 = \frac{Q_0}{n_l H b \in} \tag{1}$$

where u_0 is inlet velocity, Q_0 is inlet flow rate, n_l is number of envelopes, H is channel height, b is channel width, and ϵ is porosity of channel. This inlet velocity condition does not deviate much from values of other FO SWM simulation studies [8,9].

Each geometry is filled with unwoven net-type spacers, which is most basic and common shape in spacer research. In order to evaluate effect of spacer filament orientation, spacer angle is set to transverse and axial to inlet flow direction to observe effects of spacer angles to inlet flow direction, which are attached to top and bottom walls, respectively. All spacer filaments are assumed to have cylinder shape which is not technically true for commercial spacers but a reasonable assumption [15]. Example of envelope geometry used in this study is illustrated in Fig. 1. Dimension of commercial spacer (Toray 8040 FO element) was measured strictly to be used in the simulation. Surface of spacer filaments are treated as no-slip walls with zero velocity. A constant ambient pressure is prescribed for the outlet boundary condition.

2.2. Governing equations and modeling software

The Navier–Stokes equations were employed to describe conservation and transport processes as shown below.

The Newtonian fluid was assumed, and steady-state and laminar-based solver has been adopted. Based on results of channel and hydraulic Reynolds numbers, laminar flow regime was assured in this study. This will be further discussed in section 3.

$$\frac{\partial u}{\partial x}+\frac{\partial v}{\partial y}+\frac{\partial w}{\partial z}=0 \tag{2}$$

$$u\frac{\partial u}{\partial x}+v\frac{\partial v}{\partial y}+z\frac{\partial w}{\partial z}=-\frac{1}{\rho}\frac{\partial P}{\partial x}+\frac{\mu}{\rho}\left[\frac{\partial^2 u}{\partial x^2}+\frac{\partial^2 u}{\partial y^2}+\frac{\partial^2 u}{\partial z^2}\right] \tag{3}$$

$$u\frac{\partial u}{\partial x}+v\frac{\partial u}{\partial y}+z\frac{\partial u}{\partial z}=-\frac{1}{\rho}\frac{\partial P}{\partial x}+\frac{\mu}{\rho}\left[\frac{\partial^2 v}{\partial x^2}+\frac{\partial^2 v}{\partial y^2}+\frac{\partial^2 v}{\partial z^2}\right] \tag{4}$$

$$u\frac{\partial w}{\partial x}+v\frac{\partial w}{\partial y}+z\frac{\partial w}{\partial z}=-\frac{1}{\rho}\frac{\partial P}{\partial x}+\frac{\mu}{\rho}\left[\frac{\partial^2 w}{\partial x^2}+\frac{\partial^2 w}{\partial y^2}+\frac{\partial^2 w}{\partial z^2}\right] \tag{5}$$

where u, v, and w are velocity in x, y, and z directions, ρ is density, and P is pressure.

For the simulations in this work, ANSYS 18.0 modules were used to simulate the flow through the SWM element FO draw channels: ANSYS Geometry, ANSYS Meshing, ANSYS CFX, and ANSYS Workbench. Simulations were run in the SIMPLE (Semi-Implicit Method for Pressure Linked Equations) algorithm for pressure–velocity coupling and first-order upwind algorithm for discretization of the conservation equations. A root-mean-square residual criterion was set to 10^{-4}. The simulations were run on a PC equipped with Intel Xeon CPU E5-2620v4 eight-core 2.1 GHz processor, NVIDIA GeForce GT 710, and 128 GB of ECC registered DDR3 memory.

2.3. Hydrodynamic parameters

Effects of GL ratio and LW ratio of envelope geometries were compared based on hydrodynamic parameters presented in the following sections. In geometries of LW ratio, channel width was kept constant by adjusting central GL length accordingly. In geometries of GL ratio, however, there is difficulty to specify representative channel width and channel length because these two parameters are not constant when GL ratio changes. For this reason, channel Reynolds number was used instead of hydraulic Reynolds number, and only shear rate and pressure drop were analyzed for GL ratio comparison. Definition of channel Reynolds number is well explained in other literature [16].

Most hydrodynamic parameters considered in this study take account of different geometrical features for each geometry such as volume of fluid, porosity of channel, hydraulic diameter, and characteristic channel length. This facilitates comparing the geometries on fair terms.

2.3.1. Reynolds number

Hydraulic Reynolds number was employed to examine effects of envelope geometries on flow behaviors inside envelope geometry channel. These parameters have been widely used in literature regarding flow through spacer-filled narrow channel and showed good agreement with experimental results [10,17–21]. Hydraulic diameter, fluid and channel volume, and wetted surface area were carefully extracted from simulation results. More details on hydraulic Reynolds number can be found elsewhere in the literature [19].

$$u_{\text{eff}}=\frac{Q}{A_{\text{eff}}} \tag{6}$$

The effective velocity, u_{eff}, parameterizes the bulk average velocity of fluid in the channel. Where, volumetric flow rate, Q, divided by the effective area for flow.

$$A_{\text{eff}}=Hb\in \tag{7}$$

The effective area, A_{eff}, parameterizes the effective cross-sectional area of the spacer-filled channel.

$$\text{Re}_h=\frac{\rho u_{\text{eff}} d_h}{\mu} \tag{8}$$

2.3.2. Fanning friction factor

Fanning friction factor is dimensionless parameter normally used to estimate pressure drop in channel flow and for conduits without obstacles are defined by the following relation. However, the above equation is modified for flow with obstacles [10] such as spacer-filled narrow channels and the Fanning friction factor is related to hydraulic diameter, effective velocity, channel length, and pressure drop across the membrane. Fanning friction factor is defined as follows:

$$f=\frac{d_h \Delta P}{2\rho u_{\text{eff}}^2 L} \tag{9}$$

where d_h is the hydraulic diameter, ΔP is the channel pressure drop, ρ is the fluid density, u_{eff} is the effective velocity, and L is the channel length.

2.3.3. Specific power consumption

Specific power consumption (SPC) indicates the hydraulic energy required to overcome the fluid's channel pressure drop per unit length of the domain. SPC is defined by below equation [22].

$$\text{SPC}=u_{\text{eff}}\frac{\Delta P}{L} \tag{10}$$

where $\frac{\Delta P}{L}$ is the channel pressure drop per unit length.

2.3.4. Power number

Power number is another parameter, derived by dimensional analysis, utilized in the literature to estimate power consumption to flow through narrow spacer-filled channel [23]. The use of power number can be found in other literature [15,20,24]. The power number is expressed and related to SPC power number as follows.

$$P_n = \mathrm{SPC}\left(\frac{\rho^2 H^4}{\mu^3}\right) = \frac{\Delta P}{L}\left(\frac{u_{\mathrm{eff}}\rho^2 H^4}{\mu^3}\right) \tag{11}$$

2.3.5. Wall shear rate

Wall shear rate indicates the rate of stress that is tangentially exerted on the wall of the membrane. Efficiency of a membrane element significantly depends on the efficacy of channel geometries to increase mass transport away from the membrane surface into the bulk fluid by increasing shear rate at the membrane surface [25]. It has been reported that mass transfer is significantly enhanced in the regions of high shear rate [21]. Shear rate on membrane surface has significant improvement on permeate flux [26,27], scaling [28], and biofouling mitigation [29]. In the case of FO draw channel, dilutive concentration polarization (either internal concentration polarization or external concentration polarization) can be alleviated by high wall shear rate because higher shear rate implies a higher possibility to swipe the concentration boundary layer, thereby increasing the mass transfer and permeate flux [30].

Shear rate applied on upper and lower membrane wall was visualized in each geometry using shear rate contour and average shear rate was compared. In Ansys CFX, shear rate is calculated based on the following equations.

$$S_{ij} = \frac{1}{2}\left[\frac{\partial U_i}{\partial X_j} + \frac{\partial U_i}{\partial X_j}\right] \tag{12}$$

$$\text{Shear rate} = \left[2\frac{\partial U_i}{\partial X_j}\right]^{\frac{1}{2}} \tag{13}$$

where S_{ij} is the strain rate tensor, U_i is the flow velocity parallel to the wall, and X_j is the spatial coordinate.

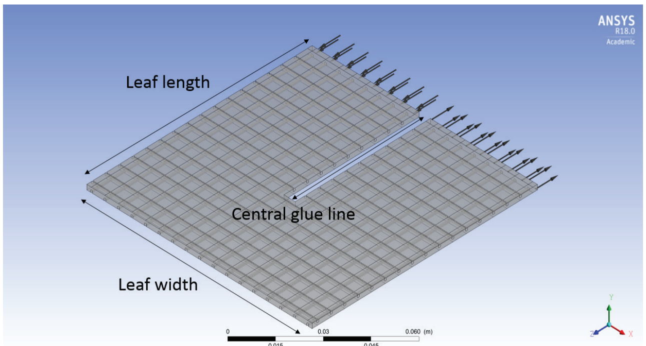

Fig. 1. Example of envelope geometry with major parameters indicated.

3. Results and discussion

3.1. Comparison of velocity volume rendering

To visualize velocity distribution in 3D spatial geometry and spots dead zone where water flow stagnates, volume-rendering function of CFX has been utilized. In volume-rendering contours, transparent region represents zero velocity while opaque region represents non-zero velocity with velocity indicating transparency and color in the given range.

Figs. 2(a), (b), and (c) illustrate velocity volume rendering with different GL ratio. At GL ratio 0.9, velocity is severely concentrated at the tip of central GL. As GL ratio decreases, velocity concentration is reduced but high-velocity zones are still present throughout all geometries with different GL ratios, even at 0.1 GL ratio, which is negligibly short central GL. Meanwhile, as evident from Figs. 2(d), (e), and (f), GL ratio also plays a decisive role in the sense that it dictates dead zone creation. In GL ratio 0.9, for instance, it is hard to identify any transparent spots through whole fluid domain, while in GL ratio 0.1 nearly about half of fluid domain seems dead zone. Dead zones are mainly formed in a vicinity of both corners on opposite sides of inlet and outlet.

Meanwhile, in volume-rendering contours of different LW ratio, there was no noticeable difference in dead zone formation found by LW ratios (Figs. 2(d), (e), and (f)). However, imbalance of velocity distribution seems getting severe as LW ratio lowers. For example, as LW ratio decreases low-velocity zone, which is indicated as dark blue, expands from both of corners in domains while area of high-velocity zone, which is indicated as light green, widens from the tip of central GL. Generally, the envelope with higher LW ratio seems more beneficial in terms of even flow distribution.

Besides observations made above, angled geometric features such as corners of envelope and tip of central GL tends to encourage creation of dead zone and excessively high-velocity zone. In this regard, there is still room for improvement of modified SWM envelope design for even flow distribution. For example, curved shape of corners and tip of central GL can be suggested.

3.2. Reynolds number

Reynolds numbers for 15 cases with different geometrical parameters were calculated and compared. For LW ratio, Re_h showed negligible deviation from each other (Table 1). This indicates that hydrodynamic condition for LW ratio comparison was sufficiently fair based on definition of hydraulic Reynolds number. Many studies compare performance of different geometries as a function of Reynolds number, however, in this study, Reynolds number is fixed as much as possible to compare geometries with different LW ratio.

However, in the comparison of GL ratio, Re_{ch} revealed linear correlation to GL ratio. Increasing Reynolds number is one of the ways to improve mass transfer in membrane channel, however, high Reynolds number means additional cost as energy losses also increase with increasing Reynolds number thus these two variables need to be interpreted together carefully [20].

In general, the Reynolds number at which the flow becomes unsteady in spacer-filled narrow channels depends on the geometry of the obstructions and can range from 200 to 600 [31]. For this reason, most literatures on 3D modeling for spacer-filled channel limits Reynolds number used as variables up to 200. As presented in Fig. 3, overall Reynolds number is around 25~30 and maximum Reynolds number is 30.48 for GL ratio 0.9. This low Reynolds numbers assure that all flow conditions in this simulation fall into laminar flow regime which is suitable for laminar solver.

3.3. Pressure drop and energy consumption

Pressure drop is a crucial hydraulic parameter because it is directly related to energy consumption in most membrane process. Fig. 4 indicates correlation between pressure drop

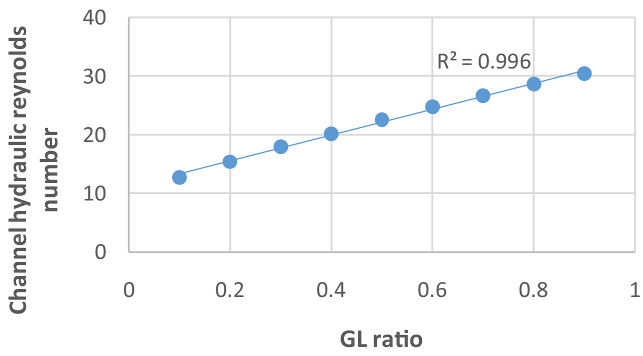

Fig. 3. Channel Reynolds number as a function of GL ratio.

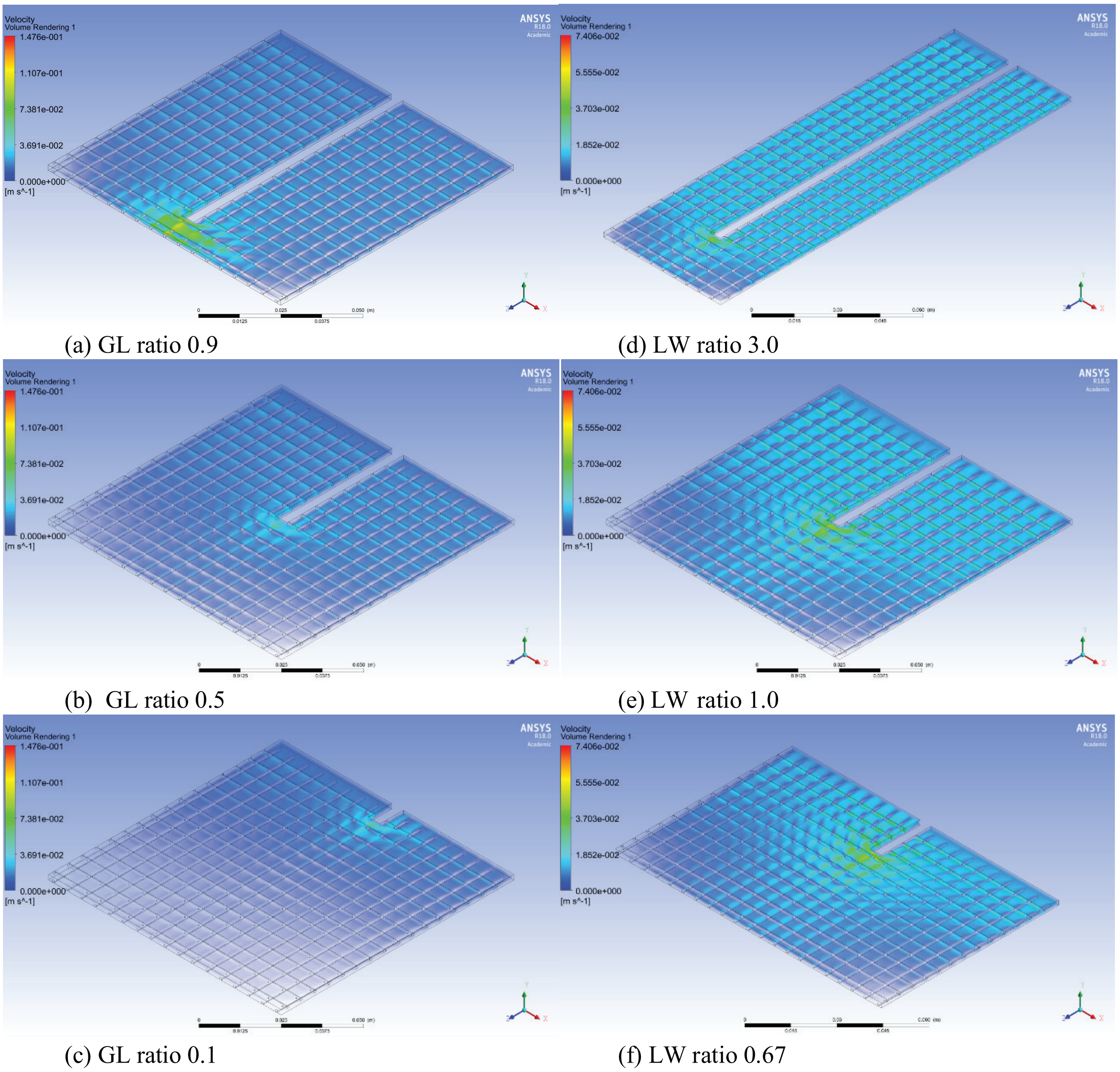

Fig. 2. Velocity volume rendering of GL ratio: (a) GL ratio 0.9, (b) GL ratio 0.5 (c) GL ratio 0.1 (d) LW ratio 3.0 (e) LW ratio 1.0 (f) LW ratio 0.67.

and GL ratio. Up to 0.6, it showed gradual increase, but after 0.6 it shifted to steep exponential growth curve. In consideration of linear increase of Reynolds number shown in the previous section, keeping GL ratio below 0.7 seems beneficial for energy efficiency of envelope unit.

In general, comparisons at the same flow condition for different geometries cannot be made by comparing a single dimensionless number because both pressure drop and pumping power are dimensional quantities and they have differing relationships to other properties. Power number and Fanning friction factor are both dimensionless numbers quantifying of energy losses through channel geometries. However, they can be differentiated by their derivation process and parameters used in equations [16]. Fig. 5 indicates power number and Fanning friction factor depending on LW ratio. Both graphs showed steep logarithmical increase up to LW ratio 2 and after that there is no significant increase of energy requirements. Both plots of power number and Fanning friction factor closely match with slight deviation after LW 1. Considering simulation results presented above, short and wide membrane envelope, especially less than LW ratio 2 is desirable to minimize energy consumption of modified SWM envelope unit. Geometrical parameters and hydrodynamic parameters in different LW ratio are show in Table 2.

Table 1
Simulation parameters used in this study

Parameter	Value
Geometrical parameters	
Filament diameter, m	0.001
Filament spacing, m	0.006
Spacer diameter (channel height), m	0.002
Flow angle of attack	0°
Envelope area, m^2	0.1
Spacer angle	0° and 90° (Angle between axial, transverse filaments, and inlet flow direction)
Porosity of channel	0.8731
Boundary conditions	
Inlet velocity, m/s	0.008768
Pressure outlet, Pa	101,325 (ambient pressure)

3.4. Shear rate on membrane walls

Fig. 6 indicates an increasing trend of average wall shear rate as a function of GL ratio. Plots of total average shear rate, average shear rate on top wall and bottom show linearly proportional tendencies. Total average shear rate is the average of shear rates on both top and bottom walls. However, it is notable that shear rate of top membrane wall shows much steeper increase rate compared with shear rate of bottom membrane wall. This also can be confirmed in shear rate contours given in Fig. 7. In Fig. 7, shear rate distributions are

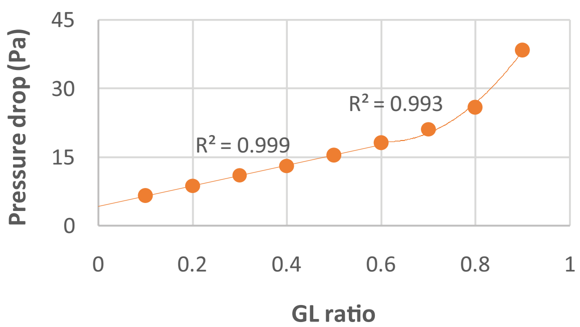

Fig. 4. Pressure drop as a function of GL ratio.

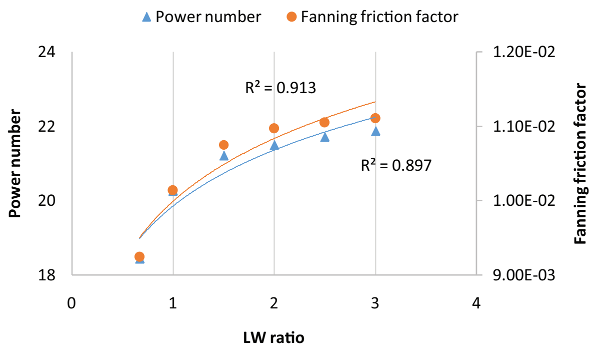

Fig. 5. Power number and Fanning friction factor as a function of LW ratio.

Table 2
Geometrical parameters and hydrodynamic parameters in different LW ratio

Parameter	LW ratio					
	3	2.5	2	1.5	1	0.67
d_h (m)	0.00233	0.00232	0.00234	0.00234	0.00233	0.00233
u_{eff} (m/s)	0.0101	0.0101	0.0101	0.0101	0.0102	0.0102
Channel length (m)	0.338	0.306	0.271	0.231	0.181	0.139
Re_h	26.3	26.2	26.5	26.5	26.5	26.6
$\frac{\Delta P}{L}$ (Pa/m)	96.02	95.52	94.92	92.84	88.32	80.34
SPC (W/m^3)	0.00097	0.000962	0.000953	0.00094	0.000898	0.000817
P_n	21.874	21.711	21.501	21.217	20.261	18.435

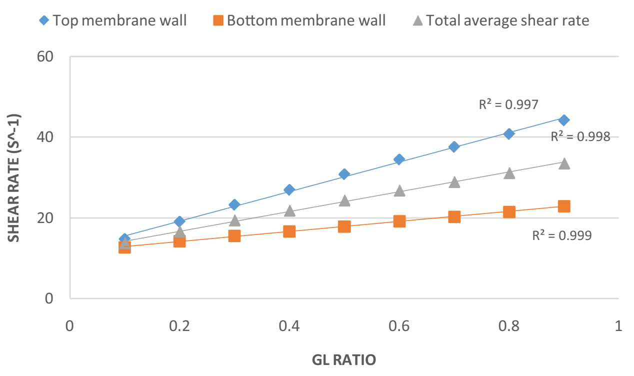

Fig. 6. Wall shear rate as a function of GL ratio.

illustrated on top walls (Figs. 7(a), (b), and (c)) and bottom walls (Figs. 7(d), (e), and (f)) with GL ratios 0.9, 0.5, and 0.1. As mentioned in Section 2.1, spacer filaments are aligned transversally and axially on top and bottom membranes, respectively. From figures above, GL ratio has a significant effect on distribution and extent of shear rate as it showed quite different appearance in shear rate contours on both walls. On top membrane walls where spacer filaments are attached parallel to main flow direction (i.e., flow direction of inlet and outlet), higher shear rates are shown. Most high shear rate zones are concentrated on areas where fluids flow along the main flow direction. On the contrary, shear rate of bottom membrane walls where filaments are set to perpendicular to the main flow direction shows lower average shear rates. Most of high shear rate zones are concentrated on areas where fluids flow transverse to the main flow direction. The high

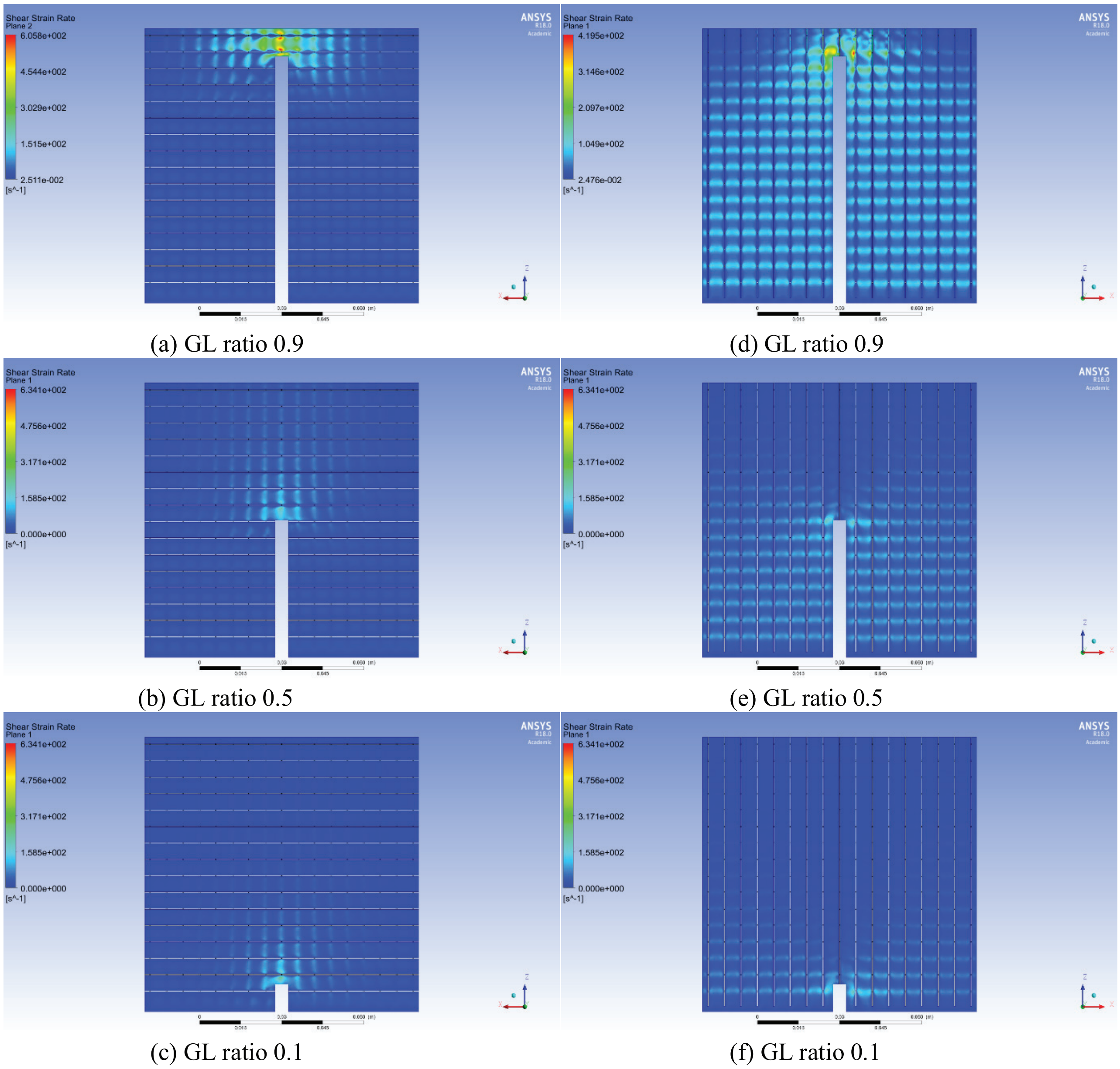

Fig. 7. Shear rate contour of GL ratio at top wall is (a) 0.9, (b) 0.5, and (c) 0.1, and GL ratio at bottom wall is (d) 0.9, (e) 0.5, and (f) 0.1.

shear rate zones also match well with high velocity zone shown in volume-rendering contours in previous section. In this respect, based on inlet and outlet flow direction, parallel spacer orientation is preferred over perpendicular orientation in terms of increasing wall shear rate and this propensity gets more intensified as GL ratio increases.

Fig. 8 presents trends of average shear rate depending on LW ratio on top and bottom membrane walls and sum of shear rate on both walls. In Fig. 9, shear rate distributions are shown on top walls (9a, (b), and (c)) and bottom walls (9d, (e), and (f)) with LW ratios 3.0, 1.0, and 0.67. Interestingly, as LW ratio increases, both graph lines reveal trends opposed to each other. Shear rate of top membrane wall increases logarithmically, while shear rate of bottom membrane wall decreases logarithmically. In both of membrane walls,

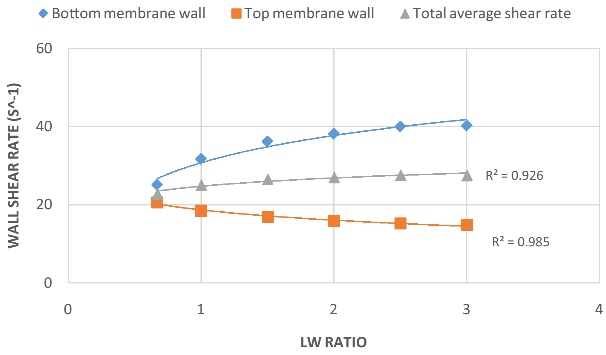

Fig. 8. Wall shear rate as a function of LW ratio.

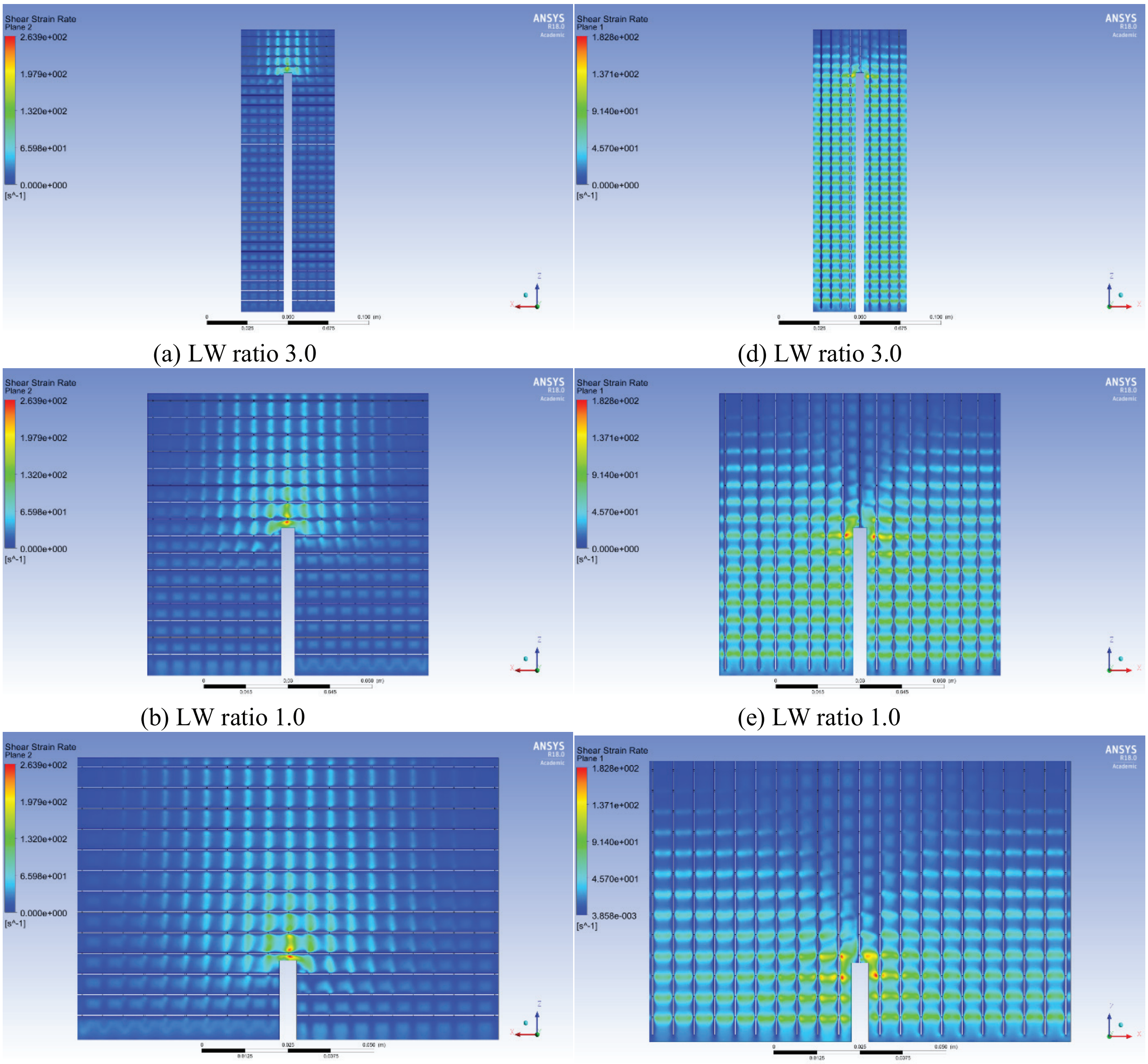

(a) LW ratio 3.0

(d) LW ratio 3.0

(b) LW ratio 1.0

(e) LW ratio 1.0

(c) LW ratio 0.67

(f) LW ratio 0.67

Fig. 9. Shear rate contour of LW ratio at top wall is (a) 3.0, (b) 1.0, and (c) 0.67, and LW ratio at bottom wall is (d) 3.0, (e) 1.0, and (f) 0.67.

variation rate of shear rate seems to become insignificant after LW ratio 2.5. This can be most likely attributed to the ratio between axial area and transversal area depending on LW ratio. Because the area in which flow direction is axial to the main flow direction increase with increasing LW ratio, higher average shear rates are induced on bottom membrane walls. On the other hand, as LW ratio decreases, which means transverse flow area increases, average shear rate on top membrane walls increases. This trend is also evident in shear rate contours in Fig. 9. It is very probable that axial spacer filaments of top membrane wall produces higher wall shear rate and high LW ratio (i.e., longer envelope geometry) creates higher shear stress due to larger axial flow area. As it is shown in shear rate contours of GL ratio, high shear rate zones in LW ratio also match well with high velocity zones in volume-rendering contours.

In conclusion, in order to boost wall shear rate, two aspects can be considered based on results from the simulations. (1) Orientation of filaments should be parallel to dominant flow direction, which is normally direction of inlet and outlet flow of envelope geometry. However, it is worth noting that transverse filaments of bottom membrane wall play a role of pushing up water flow to give high shear rate on opposite wall. (2) Envelope geometry should be narrow and long rather than wide and short. This is because larger area with axial flow is more favorable for wall shear rate when spacer filaments are set to be axial. In order to improve shear stress applied on membrane surface, spacer angle should be oriented to parallel to main flow direction. In addition, as shown in volume-rendering contours, shear rate contours also show dead zones at near-angled geometries.

4. Conclusion

3D-CFD was used to investigate the effects of modified SWM element envelope geometry on hydrodynamics inside membrane envelope depending on different GL and LW ratios. Hydrodynamic phenomena were examined by utilizing various parameters such as Reynolds number, power number, Fanning friction factor, and wall shear rate. Each parameter was calculated based on data extracted from CFD simulation. Based on the numerical results and membrane envelope geometries studied, the following conclusions can be drawn:

- Angular shape of corner of membrane envelope and tip of central GL encourage dead zone creation which has adverse effects on general membrane performance and fouling tendency.
- GL ratio higher than 0.6 should be avoided because pressure drop increases rapidly and aggravate flow distribution.
- Short and wide membrane envelope geometry is more desirable with regard to low energy consumption, while narrow and long envelope tends to create higher total average shear rate.
- Parallel alignment of spacer filaments to the main flow direction induce higher shear rates in modified SWM envelope geometry.

It should be noted that this study used impermeable boundary condition to simulate performance of unit envelope, which means mass transfer was not considered in the current simulation. Impermeable boundary condition was occasionally used because permeation velocity is negligibly lower than feed velocity in most of the membrane processes [32,33]. However, in order to examine major membrane performance such as water flux, further simulation based on permeable boundary condition is necessary.

Symbols

b	—	Channel width, m
d_h	—	Hydraulic diameter, m
f	—	Fanning friction factor
H	—	Channel height, m
L	—	Channel length, m
n_l	—	Number of envelopes
ΔP	—	Channel pressure drop, Pa
$\frac{\Delta \mathrm{P}}{\mathrm{L}}$	—	Pressure drop per length, Pa/m
P_n	—	Power number
Q_0	—	Inlet flow rate, m^3/s
Re_h	—	Hydraulic Reynolds number
S_{ij}	—	Strain-rate tensor
SPC	—	Specific power consumption, W/m^3
u_0	—	Inlet velocity, m/s
u_{eff}	—	Effective velocity, m/s
U_i	—	Displacement, m
u	—	Velocity in x direction, m/s
v	—	Velocity in y direction, m/s
w	—	Velocity in z direction, m/s
X_j	—	Spatial coordinate
ϵ	—	Channel porosity
μ	—	Dynamic viscosity, Pa s
ρ	—	Density, kg/m^3

Acknowledgment

This research was supported by a grant (code 18IFIP-B087389-05) from Industrial Facilities & Infrastructure Research Program funded by Ministry of Land, Infrastructure and Transport of Korean government.

References

[1] T.Y. Cath, A.E. Childress, M. Elimelech, Forward osmosis: principles, applications, and recent developments, J. Membr. Sci., 281 (2006) 70–87.
[2] D.L. Shaffer, J.R. Werber, H. Jaramillo, S. Lin, M. Elimelech, Forward osmosis: where are we now?, Desalination, 356 (2015) 271–284.
[3] H.K. Shon, S. Phuntsho, T.C. Zhang, R.Y. Surampalli, Forward Osmosis—Fundamentals and Applications, American Society of Civil Engineers, USA, 2015.
[4] J. Schwinge, P.R. Neal, D.E. Wiley, D.F. Fletcher, A.G. Fane, Spiral wound modules and spacers: review and analysis, J. Membr. Sci., 242 (2004) 129–153.
[5] M. Ben Boudinar, W.T. Hanbury, S. Avlonitis, Numerical simulation and optimisation of spiral-wound modules, Desalination, 86 (1992) 273–290.
[6] S. Avlonitis, W.T. Hanbury, M. Ben Boudinar, Spiral wound modules performance. An analytical solution: part II, Desalination, 89 (1993) 227–246.
[7] S. Avlonitis, W.T. Hanbury, M. Ben Boudinar, Spiral wound modules performance. An analytical solution: part I, Desalination, 89 (1993) 227–246.

[8] D.H. Jung, J. Lee, D.Y. Kim, Y.G. Lee, M. Park, S. Lee, D.R. Yang, J.H. Kim, Simulation of forward osmosis membrane process: effect of membrane orientation and flow direction of feed and draw solutions, Desalination, 277 (2011) 83–91.
[9] B. Gu, D.Y. Kim, J.H. Kim, D.R. Yang, Mathematical model of flat sheet membrane modules for FO process: plate-and-frame module and spiral-wound module, J. Membr. Sci., 379 (2011) 403–415.
[10] G. Schock, A. Miquel, Mass transfer and pressure loss in spiral wound modules, Desalination, 64 (1987) 339–352.
[11] V.V Ranade, A. Kumar, Fluid dynamics of spacer filled rectangular and curvilinear channels, J. Membr. Sci., 271 (2006) 1–15.
[12] V.V. Ranade, A. Kumar, Comparison of flow structures in spacer-filled flat and annular channels, Desalination, 191 (2006) 236–244.
[13] S. Kook, J. Kim, S.-J. Kim, J. Lee, D. Han, S. Phuntsho, W.-G. Shim, M. Hwang, H.K. Shon, I.S. Kim, Effect of initial feed and draw flowrates on performance of an 8040 spiral-wound forward osmosis membrane element, Desal. Wat. Treat., 72 (2017) 1–12.
[14] Y.C. Kim, S.J. Park, Experimental study of a 4040 spiral-wound forward-osmosis membrane module, Environ. Sci. Technol., 45 (2011) 7737–7745.
[15] V.A. Haaksman, A. Siddiqui, C. Schellenberg, J. Kidwell, J.S. Vrouwenvelder, C. Picioreanu, Characterization of feed channel spacer performance using geometries obtained by X-ray computed tomography, J. Membr. Sci., 522 (2017) 124–139.
[16] G.A. Fimbres-Weihs, D.E. Wiley, Review of 3D CFD modeling of flow and mass transfer in narrow spacer-filled channels in membrane modules, Chem. Eng. Process. Process Intensif., 49 (2010) 759–781.
[17] G.A. Fimbres-Weihs, D.E. Wiley, Numerical study of mass transfer in three-dimensional spacer-filled narrow channels with steady flow, J. Membr. Sci., 306 (2007) 228–243.
[18] G.A. Fimbres-Weihs, D.E. Wiley, Numerical study of two-dimensional multi-layer spacer designs for minimum drag and maximum mass transfer, J. Membr. Sci., 325 (2008) 809–822.
[19] O. Kavianipour, G.D. Ingram, H.B. Vuthaluru, Investigation into the effectiveness of feed spacer configurations for reverse osmosis membrane modules using Computational Fluid Dynamics, J. Membr. Sci., 526 (2017) 156–171.
[20] A. Saeed, Effect of feed channel spacer geometry on hydrodynamics and mass transport in membrane modules, PhD Thesis, Department of Chemical Engineering, School of Chemical and Petroleum Engineering, Curtin University, 2012.
[21] G.A. Fimbres-Weihs, D.E. Wiley, D.F. Fletcher, Unsteady flows with mass transfer in narrow zigzag spacer-filled channels: a numerical study, Ind. Eng. Chem. Res., 45 (2006) 6594–6603.
[22] A. Storck, D. Hutin, Energetic aspects of turbulence promotion applied to electrolysis processes, Can. J. Chem. Eng., 58 (1980) 92–102.
[23] F. Li, W. Meindersma, A.B. De Haan, T. Reith, Optimization of commercial net spacers in spiral wound membrane modules, J. Membr. Sci., 208 (2002) 289–302.
[24] Y.L. Li, K.L. Tung, CFD simulation of fluid flow through spacer-filled membrane module: selecting suitable cell types for periodic boundary conditions, Desalination, 233 (2008) 351–358.
[25] A.R. Da Costa, A.G. Fane, C.J.D. Fell, A.C.M. Franken, Optimal channel spacer design for ultrafiltration, J. Membr. Sci., 62 (1991) 275–291.
[26] S.S. Bucs, A.I. Radu, V. Lavric, J.S. Vrouwenvelder, C. Picioreanu, Effect of different commercial feed spacers on biofouling of reverse osmosis membrane systems : a numerical study, Desalination, 343 (2014) 26–37.
[27] A.I. Radu, J.S. Vrouwenvelder, M.C.M. Van Loosdrecht, C. Picioreanu, Modeling the effect of biofilm formation on reverse osmosis performance : flux, feed channel pressure drop and solute passage, J. Membr. Sci., 365 (2010) 1–15.
[28] A.I. Radu, L. Bergwerff, M.C.M. Van Loosdrecht, C. Picioreanu, A two-dimensional mechanistic model for scaling in spiral wound membrane systems, Chem. Eng. J., 241 (2014) 77–91.
[29] J.S. Vrouwenvelder, D.A.G. Von Der Schulenburg, J.C. Kruithof, M.L. Johns, M.C.M. Van Loosdrecht, Biofouling of spiral-wound nanofiltration and reverse osmosis membranes : a feed spacer problem, Water Res., 43 (2009) 583–594.
[30] M. Park, J.H. Kim, Numerical analysis of spacer impacts on forward osmosis membrane process using concentration polarization index, J. Membr. Sci., 427 (2013) 10–20.
[31] J. Schwinge, D.E. Wiley, D.F. Fletcher, Simulation of unsteady flow and vortex shedding for narrow spacer-filled channels, Ind. Eng. Chem. Res., 42 (2003) 4962–4977.
[32] M. Shakaib, S.M.F. Hasani, M. Mahmood, Study on the effects of spacer geometry in membrane feed channels using three-dimensional computational flow modeling, J. Membr. Sci., 297 (2007) 74–89.
[33] M. Shakaib, S.M.F. Hasani, M. Mahmood, CFD modeling for flow and mass transfer in spacer-obstructed membrane feed channels, J. Membr. Sci., 326 (2009) 270–284.